AFRL-RQ-WP-TP-2014-0168

SERPENTINE DIFFUSER PERFORMANCE WITH EMPHASIS ON FUTURE INTRODUCTION TO A TRANSONIC FAN (POSTPRINT)

Chase A. Nessler, William W. Copenhaver, and Michael G. List

Turbomachinery Branch
Turbine Engine Division

JANUARY 2013

AIR FORCE RESEARCH LABORATORY
AEROSPACE SYSTEMS DIRECTORATE
WRIGHT-PATTERSON AIR FORCE BASE, OH 45433-7542
AIR FORCE MATERIEL COMMAND
UNITED STATES AIR FORCE

NOTICE AND SIGNATURE PAGE

Using Government drawings, specifications, or other data included in this document for any purpose other than Government procurement does not in any way obligate the U.S. Government. The fact that the Government formulated or supplied the drawings, specifications, or other data does not license the holder or any other person or corporation; or convey any rights or permission to manufacture, use, or sell any patented invention that may relate to them.

This report was cleared for public release by the USAF 88th Air Base Wing (88 ABW) Public Affairs Office (PAO) and is available to the general public, including foreign nationals.

Copies may be obtained from the Defense Technical Information Center (DTIC) (http://www.dtic.mil).

AFRL-RQ-WP-TP-2014-0168 HAS BEEN REVIEWED AND IS APPROVED FOR PUBLICATION IN ACCORDANCE WITH ASSIGNED DISTRIBUTION STATEMENT.

*//Signature//
STEVEN L. PUTERBAUGH
Work Unit Manager
Turbomachinery Branch
Turbine Engine Division

//Signature//
CHARLES W. STEVENS, Chief
Turbomachinery Branch
Turbine Engine Division

//Signature//
ROBERT D. HANCOCK
Principal Scientist
Turbine Engine Division
Aerospace Systems Directorate

This report is published in the interest of scientific and technical information exchange, and its publication does not constitute the Government's approval or disapproval of its ideas or findings.

*Disseminated copies will show "//Signature//" stamped or typed above the signature blocks.

REPORT DOCUMENTATION PAGE

Form Approved
OMB No. 0704-0188

1. REPORT DATE *(DD-MM-YY)*	2. REPORT TYPE	3. DATES COVERED *(From - To)*
January 2013	Conference Paper Postprint	01 June 2012 – 01 December 2012

4. TITLE AND SUBTITLE
SERPENTINE DIFFUSER PERFORMANCE WITH EMPHASIS ON FUTURE INTRODUCTION TO A TRANSONIC FAN (POSTPRINT)

5a. CONTRACT NUMBER
In-house

5b. GRANT NUMBER

5c. PROGRAM ELEMENT NUMBER
62203F

6. AUTHOR(S)
Chase A. Nessler, William W. Copenhaver, and Michael G. List

5d. PROJECT NUMBER
3066

5e. TASK NUMBER
N/A

5f. WORK UNIT NUMBER
Q0GE

7. PERFORMING ORGANIZATION NAME(S) AND ADDRESS(ES)
Turbomachinery Branch (AFRL/RQTT)
Turbine Engine Division
Air Force Research Laboratory, Aerospace Systems Directorate
Wright-Patterson Air Force Base, OH 45433-7542
Air Force Materiel Command, United States Air Force

8. PERFORMING ORGANIZATION REPORT NUMBER
AFRL-RQ-WP-TP-2014-0168

9. SPONSORING/MONITORING AGENCY NAME(S) AND ADDRESS(ES)
Air Force Research Laboratory
Aerospace Systems Directorate
Wright-Patterson Air Force Base, OH 45433-7542
Air Force Materiel Command
United States Air Force

10. SPONSORING/MONITORING AGENCY ACRONYM(S)
AFRL/RQTT

11. SPONSORING/MONITORING AGENCY REPORT NUMBER(S)
AFRL-RQ-WP-TP-2014-0168

12. DISTRIBUTION/AVAILABILITY STATEMENT
Approved for public release; distribution unlimited.

13. SUPPLEMENTARY NOTES
PA Case Number: 88ABW-2012-6479; Clearance Date: 12 Dec 2012.

The conference paper was presented at the 51st AIAA Aerospace Sciences Meeting, including the New Horizons Forum and Aerospace Exposition, held in Grapevine, Texas from January 07 through 10, 2013 and was published by AIAA proceedings of the conference, Paper Number AIAA 2013-0219.

14. ABSTRACT
A serpentine diffuser for embedded propulsion systems was characterized in terms of pressure recovery and total pressure distortion generation within the discharge flow field. A new experimental facility was constructed and also characterized for this investigation to provide detailed, high fidelity measurements. Diffuser performance was characterized for five different Mach numbers with 195 axial and circumferential static pressure measurements within the diffuser flow path. Pressure distortion at the diffuser discharge was quantified with detailed static and steady total pressure measurements at the 17-inch aerodynamic interface plane (AIP). These measurements were acquired using eight total pressure rakes with ten radial probes each while rotating the diffuser in 5-degree increments, yielding highly detailed pressure distortion measurements at the AIP. The wall static pressure plots of diffuser performance display signs of detached flow along the wall at design conditions. Total pressure contour plots at the AIP show a concentrated pressure distortion pattern at the top center exit of the diffuser resulting in an overall recovery factor of 0.983. Distortion descriptors are presented and discussed.

15. SUBJECT TERMS
diffuser, transonic fan, distortion

16. SECURITY CLASSIFICATION OF:			17. LIMITATION OF ABSTRACT:	18. NUMBER OF PAGES	19a. NAME OF RESPONSIBLE PERSON (Monitor)
a. REPORT	b. ABSTRACT	c. THIS PAGE			Steven L. Puterbaugh
Unclassified	Unclassified	Unclassified	SAR	24	19b. TELEPHONE NUMBER *(Include Area Code)* N/A

Serpentine Diffuser Performance with Emphasis on Future Introduction to a Transonic Fan

Chase A. Nessler[1], William W. Copenhaver[2], and Michael G. List[1]
Air Force Research Laboratory, WPAFB, OH, 45433

A serpentine diffuser for embedded propulsion systems was characterized in terms of pressure recovery and total pressure distortion generation within the discharge flow field. A new experimental facility was constructed and also characterized for this investigation to provide detailed, high fidelity measurements. Diffuser performance was characterized for five different Mach numbers with 195 axial and circumferential static pressure measurements within the diffuser flow path. Pressure distortion at the diffuser discharge was quantified with detailed static and steady total pressure measurements at the 17 inch Aerodynamic Interface Plane (AIP). These measurements were acquired using 8 total pressure rakes with ten radial probes each while rotating the diffuser in five degree increments, yielding highly detailed pressure distortion measurements at the AIP. The wall static pressure plots of diffuser performance display signs of detached flow along the wall at design conditions. Total pressure contour plots at the AIP show a concentrated pressure distortion pattern at the top center exit of the diffuser resulting in an overall recovery factor of 0.983. Distortion descriptors are presented and discussed.

I. Introduction

A. Background

Next generation aircraft are utilizing integrated airframes that contain embedded propulsion systems. These types of airframes require even more geometrically complex diffusing S-ducts than before, to condition the airflow from the airframe inlet to the embedded engine, as shown in Figure 1. Shorter airframes that yield increased thrust to weight ratios have led to a new generation of S-ducts that are ultra-compact and characterized as serpentine diffusers. Serpentine diffusers vary from S-ducts by the addition of a third flow field turn back toward the original inlet centerline, resulting in minimal vertical offset in the through-flow direction. In addition to this, serpentine diffusers contain a continuous transitioning cross-section from a unique inlet cross-sectional shape to a circular cross-section at the exit. Compact serpentine diffusers include highly curved surfaces which, in combination with a significant amount of diffusion, generate multiple unsteady vortical flow structures on the scale of the fan blade spacing. These structures impinge upon the front fan stages of the turbine engine, creating significant diffuser/fan interaction.

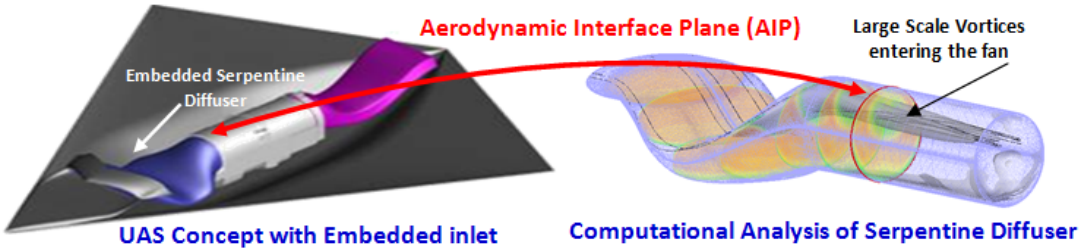

Figure 1. Rendition of embedded propulsion installation in UAS

[1] Aerospace Engineer, Propulsion Directorate, 1950 Fifth St, Member AIAA.
[2] Aerospace Engineer, Propulsion Directorate, 1950 Fifth St, Fellow AIAA.

Inlet S-ducts have been used in both military and commercial aircraft on many different air platforms. Some examples of these aircraft include the General Dynamics F-16, McDonnell-Douglas F-18, and the Boeing 727. The complex flows that develop due to the centerline curvature, changes in cross-sectional shape, and increasing area; have all been well documented [1-4]. It has been shown, both experimentally and computationally, that the centerline curvature of an S-duct along with the changes in cross sectional shape, generates strong cross-stream pressure gradients that produce secondary flows. These secondary flows develop axially into counter-rotating vortices [5-8]. In addition to the secondary flows, a streamwise adverse pressure gradient exists from the increasing cross sectional area, which can lead to flow separation within the S-duct. The resulting flow quality at the exit of the duct and entering the first stage of the compressor is degraded by flow non-uniformity (distortion) and a reduction in total pressure. The effect of flow non-uniformity and a reduced total pressure recovery is a decrease in compressor stall margin and efficiency for a given engine.

In an extensive study by Rabe [9] with the Lockheed Martin STRICT serpentine diffuser, the diffuser geometry was described as two S-ducts connected at the second turn, as shown in Figure 2. This interpretation of the duct geometry agreed with the experimental results in that two sets of counter-rotating vortices were generated, one from each S-duct. Although literature on serpentine diffusers is limited, the flow physics involved in these types of ducts is very similar to that in an S-duct. With next generation aircraft imposing complex diffusing geometries with shorter axial lengths, it is expected that the flow at the exit of a serpentine diffuser will contain more flow distortion, vorticity, and more losses than previous S-ducts.

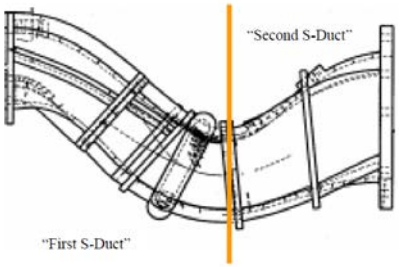

Figure 2. STRICT serpentine diffuser [9]

The purpose of this paper is to present the results from the first phase of a multi-phase research program to investigate the flow characteristics of a typical, ultra-compact, serpentine diffuser and evaluate its effects on the performance of a transonic fan. Initial results of diffuser wall static pressure measurements along with steady state total pressure measurements at the Aerodynamic Interface Plane (AIP) located near the exit of the diffuser are presented. Diffuser performance is characterized by the measured total pressure recovery and standardized distortion descriptors, outlined by the Society of Automotive Engineers (SAE) Aerospace Recommended Practice (ARP) 1420 document [10-11]. In addition to these results, a detailed description is given of the new research facility that was constructed for this research program to investigate serpentine diffusers in isolation of the compression system, with the overall goal of coupling the diffuser research article to a transonic fan.

B. Program Overview

Embedded inlet systems are enabling technologies to assure survivability and effectiveness of both manned and Unmanned Arial Systems (UAS). Embedded inlet systems will be highly irregular, compact, and serpentine in nature. The Air Force Research Laboratory (AFRL) located at Wright-Patterson Air Force Base (WPAFB) has undertaken an extensive multi-phase research program with the objectives to 1) quantify the wall static pressure field within the diffuser, both in isolation and coupled with the fan, as a benchmark data set for future computational validations, 2) experimentally and computationally resolve a highly unsteady velocity field at the AIP of a serpentine diffuser in both an isolated configuration and coupled with a transonic fan, 3) describe the impact of identified flow structures on fan performance with special emphasis placed on inlet swirl, and 4) develop methods in both the fan and diffuser to minimize the influence of the vorticity and pressure distortion on propulsion system performance. These scientific and technical challenges will be addressed in a four phase approach. The first phase consists of an evaluation of isolated diffuser performance through measurements of: diffuser wall statics, steady and unsteady pressure distortion field at the AIP, and Particle Image Velocimetry (PIV) also at the AIP. In Phase II, the steady state total pressure profile measured in Phase I will be simulated through distortion screens in-front of a transonic fan. The influence of the pressure distortion alone on fan performance will be quantified. The research compressor chosen to carry out this program is a single stage transonic fan. The rotating fan blade row has no IGVs

and is a typical low aspect ratio fan blade representative of most high performance fan jet applications with a relevant scale of 17 inches in diameter. Phase III of the program will demonstrate fan performance with the serpentine diffuser positioned in front of the transonic fan. In this phase, the interaction that will occur as a result of the close coupling of fan and diffuser will be investigated in detail. Fan performance will be quantified and compared to that in Phase II in which the swirl component of the flow field was not simulated. Finally, Phase IV of the program will involve the demonstration of flow control techniques in the coupled diffuser/fan configuration to mitigate detrimental interaction effects on the fan. Throughout this research program, an extensive computational effort will be undertaken to model and quantify the flow physics in each phase. This paper will focus on overall research capabilities and the results obtained to date of Phase I efforts.

II. Experimental Setup

A. Experimental Facility

The experimental facility used to conduct this research is the Compressor Aero Research Laboratory (CARL) located at WPAFB in Dayton, Ohio. The CARL is contained within an 82 ft. x 29 ft. research cell that houses a 6,000 hp, 22,000 RPM capable drive system used for open loop fan and compressor research. This research cell also contains a 6' diameter pipe connection to the Component Research Air Facility (CRAF) gas turbo exhausters with an exhaust capability of over 100,000 CFM at a minimum pressure of 11 inches of mercury [12]. As part of this research program, this exhaust capability was utilized for first time in the CARL, and a new experimental facility was constructed specifically as an in-flow static test facility.

Although the design of this new static test facility was in parallel with the design and procurement of the diffuser research article, the facility was to be adaptable for different configurations and uses. A future use of this facility includes annular cascade testing and was named as the Annular Cascade Facility (ACF).

The CRAF exhauster connection protrudes through the CARL floor at a fixed location based on previous engine research programs. Since space was limited within the research cell, the ACF was designed with a vertical test configuration. The existing 6 ft. diameter pipe leading to the turbo exhauster complex was adapted to allow for a 17 inch diameter mating section for the diffuser research article. This adaptor section was designed to be 10 duct diameters in length before the transition back to the 6 ft. diameter pipe to assure minimal downstream influence on the diffuser exit plane measurements. In order to allow for closed-loop feedback control of the flow rate entering the ACF, a flow rate trim station was installed and optimized. With this trim station in place, the overall inlet Mach number to the serpentine diffuser could be controlled to within ±0.5%. A 3-D CAD model of the ACF is shown in Figure 3.

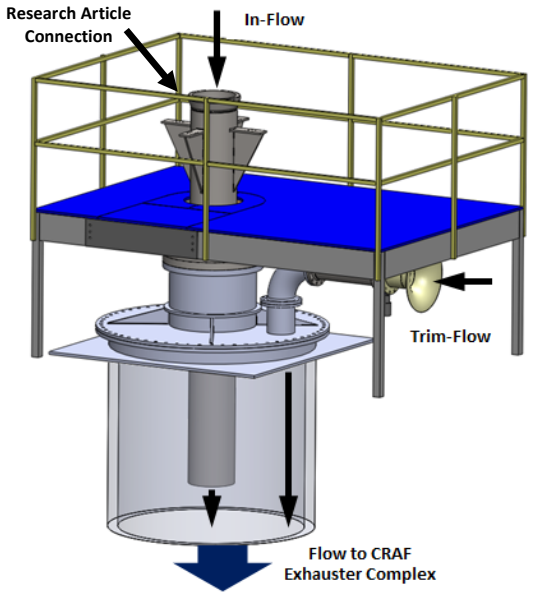

Figure 3. 3-D CAD representation of the ACF

B. Serpentine Diffuser Research Article

The serpentine diffuser research article's geometry is non-proprietary and broadly applicable for subsonic diffusers, with a design throat Mach # 0.65. The area ratio from inlet to exit is 1.19 with an engine face offset (inlet center line to exit centerline) of 20%. It has an aggressive length to diameter ratio and limited line of sight characteristics.

The ability to integrate the diffuser research article to the compressor facility research fan was a primary design constraint. The transonic fan flow path diameter of 17 inches was used to scale the diffuser geometry with the matching exit diameter. In order to appropriately couple the diffuser to the existing compressor facility flow path hardware, it was decided to utilize an embedded bellmouth to guide the flow into the diffuser. This was accomplished by using a short radius bellmouth, and immersing the bellmouth in the 48 inch diameter flow conditioning barrel used for the compressor research article. For consistency between the isolated experiments in the ACF and the coupled experiment in the compressor facility, a similar flow conditioning barrel was designed and procured for the static test. By doing this, the same inlet flow conditions entering the diffuser will be achieved in both the static and coupled experiments. A 3-D CAD representation of the facility layout is shown in Figure 4.

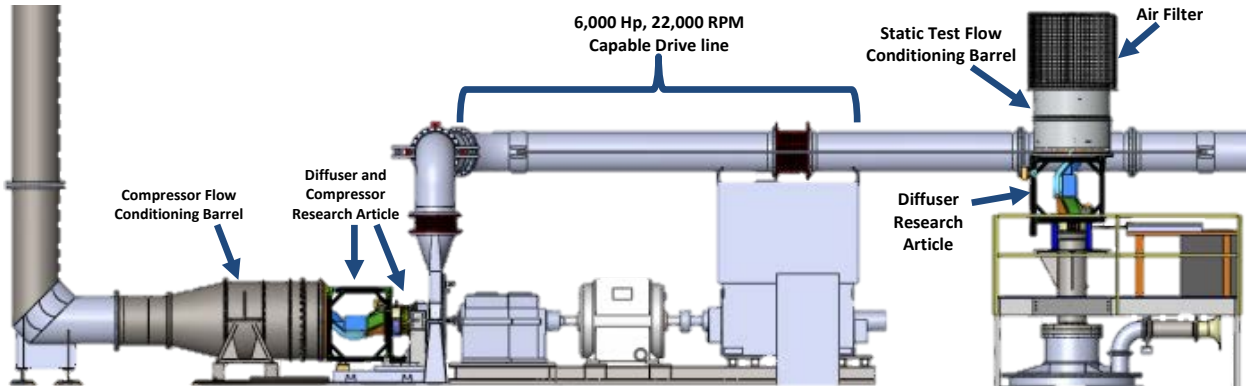

Figure 4. Compressor Aero Research Laboratory (CARL Facility)

The diffuser research article was developed to maximize the potential to understand the complex flow field within, as well as quantify the exit conditions. Shown in Figure 5, it is constructed of aluminum to assure dimensional stability making it applicable for long term research studies. It is positioned within a fixed "space frame" to allow it to be rotated to within ± .1 degree of command location within the frame through a gear drive system. This rotational capability was required to accommodate the fixed reference frame measurements that exist on the research fan to which it will ultimately be coupled. Fan performance with inlet distortion can only be quantified if measurements are made at circumferential increments that are much smaller than the extent of the distortion. This can be accommodated by using a circumferentially traversing rake system at the exit of the fan; or in this case by incrementally rotating the distortion created by the diffuser in front of the fan which has fixed exit performance rakes. In addition, during the isolated diffuser phase of this research program, this rotational capability will be used to increase the density of the measurements made from the diffuser exit fixed rake system.

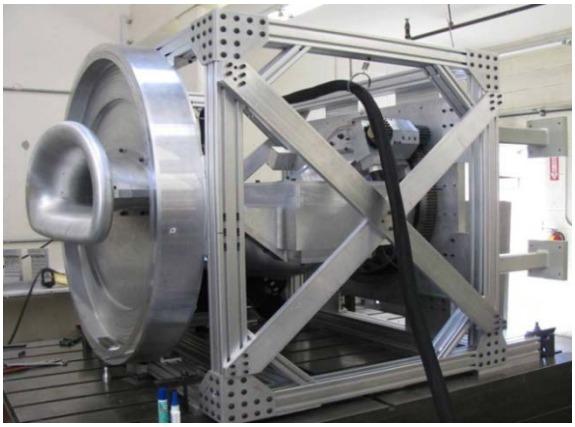

Figure 5. Serpentine diffuser research article

The diffuser was manufactured in 4 segments, assembled, and blended at the interfaces to assure a smooth flow path profile. The segments are defined as Upper Forward Diffuser (UFD), Lower Forward Diffuser (LFD), Upper Aft Diffuser (UAD), and Lower Aft Diffuser (LAD). The diffuser was also designed with a removable section within the UFD that spans the axial region of maximum static pressure rise within the diffuser. This removable section is identified as the Flow Control Plug (FCP). These designations; UFD, LFD, UAD, LAD and FCP are used to identify wall static measurement locations within the diffuser. The FCP for this part of the research program was a blank plug instrumented only with wall static pressure measurements. However, several plug replacements with different flow control mechanisms have been designed for future research.

As previously discussed, a 48" diameter flow conditioning barrel was located upstream of the diffuser entrance in the static test to help guide the flow into the diffuser bellmouth. At the entrance of the flow conditioning barrel was a 48" short radius bellmouth followed by a 4 inch thick section of ¼" web honeycomb section to straighten the flow entering the flow conditioning barrel. Downstream of the flow straightening section were two 12 mesh flow conditioning screens to reduce free stream turbulence and create a uniform velocity field across the diameter of the flow conditioning barrel. The velocity distribution across the flow conditioning barrel was measured at the same axial location of inlet temperature and pressure measurements. The velocity was uniformly distributed within ±15% from the center to the outer walls of the flow conditioning barrel and the turbulence was measured at 2%. Within the flow conditioning barrel, 22 thermocouples were positioned 13 inches upstream of the diffuser bellmouth and arranged at centers of equal area. These thermocouple readings were averaged and used to establish diffuser inlet temperature. Along with these temperature measurements, 4 wall static measurements near the location of the thermocouples were used to establish inlet total pressure. Velocities within the flow barrel were nominally 70 ft/sec allowing for the static pressure to be used as the total pressure and still remain well within the measurement uncertainty of the overall pressure measurement system. This was the same arrangement that has been used in the compressor facility to determine inlet temperature and pressure. The diffuser research article installed in the ACF with the flow conditioning barrel is shown in Figure 6.

Figure 6. Detailed configuration of isolated diffuser test setup on the ACF

C. Diffuser Instrumentation

The diffuser contains a total of 195 wall static pressure measurements, 0.042 inch diameter and blended flush to the diffuser walls for documenting internal performance. At a common circumferential location, 97 evenly distributed axial static pressure taps exist; 50 at bottom dead center of the diffuser and 47 at top dead center. Along the top of the diffuser in the upper aft section, a viewing window was placed to allow for future optical flowfield measurement techniques to be used. This section prohibited the installation of static pressures along its axial length. The remaining 98 static pressure measurements were located at four different axial locations within the diffuser and distributed circumferentially along the diffuser wall. Those locations were at the entrance to the diffuser near the minimum area (throat); forward and aft on the flow control plug; and near the exit to the diffuser.

The diffuser was designed to accommodate multiple exit measurement case rings where the AIP was established. The AIP for the diffuser was 2.54 inches downstream of the diffuser exit, and 1/3 of a duct diameter upstream of the fan research article stack axis. There are currently three cases of equal axial length available to independently position at the exit; 81 element time-averaged total pressure rake case; 40 element time-resolved total pressure rake case with an interchangeable five element 5-hole probe rake, and an optical diagnostic (PIV) case. Data presented in this paper were obtained with the time-averaged total pressure rake case which will be described in detail here. Figure 7 shows the time averaged total pressure rake case used to acquire the data presented. The figure also shows the case installed at the exit of the diffuser on the ACF.

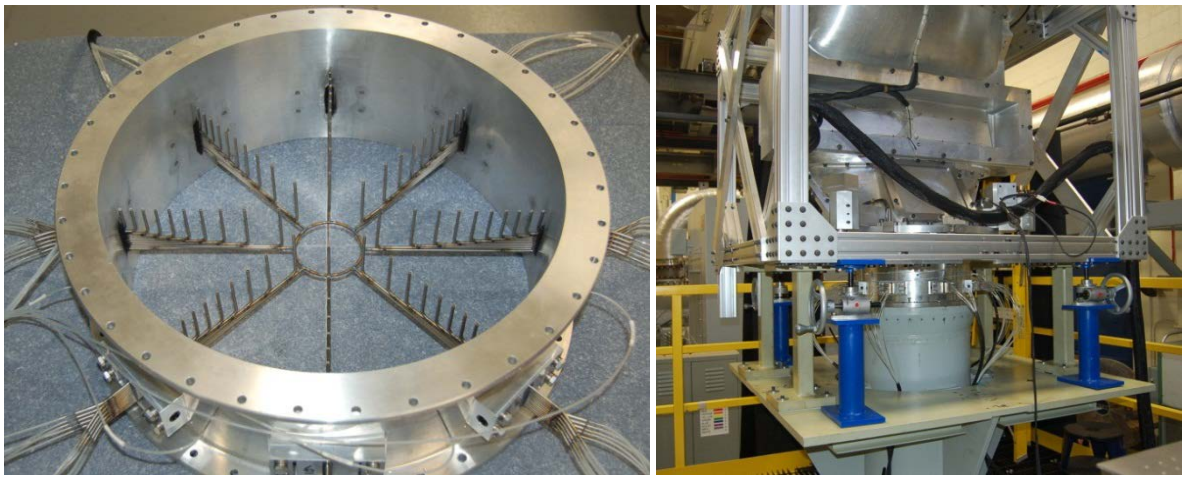

Figure 7. Time averaged total pressure rake case (Left). Rake case installed in ACF (Right)

This case is configured with 8 rakes evenly spaced around the circumference of the diffuser exit with ten probes on each rake at radial centers of equal area. In addition, a single probe was positioned at the center of the case for further radial profile definition. These 81 total pressure measurements along with diffuser rotational capability were used to establish the exit total pressure profile in unprecedented detail at this scale. With nine diffuser positions at five degree increments between each rake, the equivalent of 721 exit steady total pressure measurements are provided at the exit of the diffuser. In addition, eight wall static pressures were positioned circumferentially between the rakes at the same axial plane (AIP) of the total pressure probe tips.

The probes were constructed from stainless steel tubing with 0.027 inch inside diameter and 0.625 inch outside diameter, producing a total blockage of approximately 4% of the flow path. Each probe tip had an internal bevel angle of 26° at the AIP plane which gave a yaw tolerance of ± 25° at a Mach number of 0.62 (Gracey [13]).

D. Data Acquisition

Pressure data was acquired through a 256 channel Scanivalve pressure measurement system. This system will also be used when the diffuser is coupled to the fan; thereby eliminating any bias effects between the two configurations. The AIP rake total pressures were measured with 5 modules of 16-channels each, 5 psid maximum range transducers, while all other pressures were measured with 15 psid maximum range transducers. All pressure transducers were referenced to atmospheric pressure. With the steady total pressure rake case installed, it was not possible to measure all existing (195) static pressures on the diffuser. When AIP total pressure data was being acquired, a subset of the wall static pressures was selected for measurement. This subset contained all of the

diffuser throat and axial static pressures. Separate test periods were required to obtain data from all the diffuser static measurement locations. As a result of this requirement for multiple experimental runs and the need to evaluate diffuser exit conditions with at least 3 different exit measurement cases, repeatability of the measurements must be considered.

Flowfields within serpentine diffusers typically have unsteady components that can be sensed with modern day steady-state data acquisition systems. The measurement scan rates of these steady-state systems are high enough to capture components of unsteadiness. Through a series of experiments, an optimum balance was achieved between the time to acquire a "steady-state" data point and achievement of maximum steady state repeatability. To obtain this balance, the data system was set to acquire a running average of 600 individual measurements reported from the pressure sensing system. To obtain this running average value, a time period of approximately 3 minutes was required to obtain a steady-state data point. Therefore all reported steady data is based on the arithmetic mean value of 600 measurements acquired by the Scanivalve system. With this approach, the repeatability of the data presented is within ±1.5 % of the measured (differential) value.

Twenty four evenly spaced circumferential static pressure measurements, 2.5 inches downstream of the minimum area "throat" section of the diffuser were used to establish throat Mach number. It was not possible to place these measurements at the minimum area location due to mechanical constraints imposed by the bolting flanges of the diffuser and the ability to rotate. Numerical averages of these measurements were used to quantify the throat Mach number for diffuser inlet condition control with the trim feedback control (trim flow) identified in Figure 3.

III. Results

A. Axial and Circumferential Wall Static Pressure Measurements

Wall static pressure measurements were obtained for two axial and four circumferential traces for five different Mach numbers. All wall static pressure data has been normalized with respect to the inlet total pressure measured within the flow conditioning barrel. Circumferential data is plotted starting from the middle left corner looking downstream and progresses clockwise around the diffuser flow path. As mentioned before, each data point is a mean value with a repeatability of (+/-) 1.5% of the measured value.

Figure 8 is a plot of the circumferential static pressure distribution along the experimental throat of the diffuser. The axial location of the throat with respect to the diffuser cross-section is shown in Figure 9 and 10. The static wall taps contained within the upper and lower forward sections of the diffuser are indicated. The geometrical shape of the diffuser at this cross-section consists of a relatively flat bottom section and a circular top section. At this axial location, the flow has exited the short radius bellmouth and just entered the diffuser. The pressure profile shows the highest wall static pressure located at the center of the upper surface with a symmetric distribution of lower pressure on either side. The lower diffuser section which is relatively flat at this cross-section, exhibits a flat low pressure profile along the surface. The wall static pressure at the bottom of the diffuser does not begin to increase until it reaches the sides, where it transitions to a circular profile. This flat profile is expected to contain the lowest static pressure relative to the top section, in anticipation of the downward turn the diffuser geometry makes and the need for the flow to accelerate around it.

The effect of Mach number is shown as a shift in static pressure as expected for the attached flow along this surface. The extent of the shift due to the change in Mach number is more pronounced on the bottom surface which has a higher velocity than the top surface. For the Mach numbers tested, the change in Reynolds number is minimal and it is expected the Mach number variation will have little impact on the flow physics.

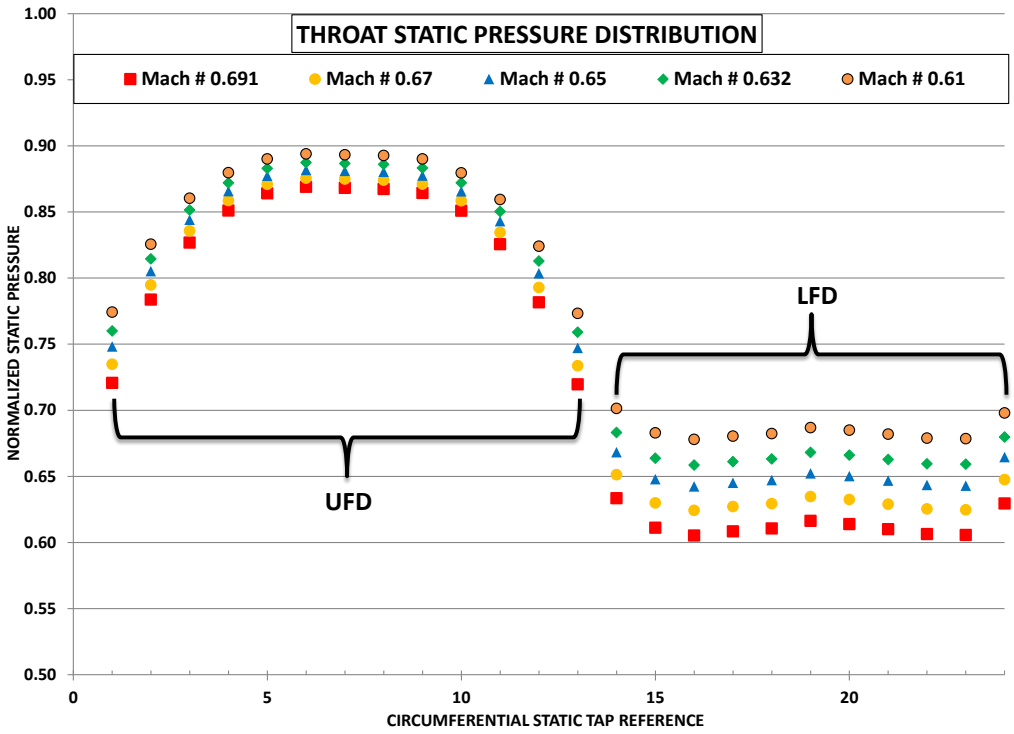

Figure 8. Circumferential wall static pressure distribution at the experimental throat

The axial wall static pressure distribution along the top dead center and bottom dead center of the diffuser is presented in Figure 9 and 10 respectively. In both figures, an axial cross-section of the diffuser upper and lower surface is shown with a normalized axial length. The locations of the four circumferential measurement planes are indicated along with the locations of the static pressure taps within the flow path.

The axial static pressure distribution is expected to exhibit similar flow physics seen in duct flows with centerline curvature, changing cross-sectional shape, and a diffusing cross-sectional area as described in previous studies. Schlicting [14] along with other investigators, were able to describe the fluid motion in a bend and the necessity of a pressure gradient being established to provide the inward acceleration. This causes an increase in static pressure on the outer wall relative to the static pressure along the inner wall. This phenomenon is easily seen in the axial static pressure distribution on both the upper and lower surfaces.

For this diffuser geometry, the incoming air is initially turned downward. In this first bend, the top surface is on the outside of the turn and acts as the pressure surface. The pressure distribution initially indicates an adverse pressure gradient coming in through the throat and impinging upon the first turn. As the flow progresses around this first turn, the pressure gradient becomes favorable. The static pressure begins to decrease along this surface as the flow begins to accelerate in anticipation of the second turn. Near the middle of the second turn, the pressure gradient changes signs again and becomes adverse as the flow comes around the second turn and the upper surface is now on the inside of the turn (suction surface).

The static pressure continues to increase (boundary layer should thicken) along the top surface in the second turn until the profile flattens out at an axial location of 0.48. This is believed to indicate separation. In studies by Wellborn et al. [3] and Valkili et al. [7], the constant static pressure profiles were shown to agree with the flow visualization of where the flow separated along the duct. In these studies, the static pressure eventually continued to increase, but occurred forward of the reattachment point as a result of the diffusion taking place in the duct. Although the static pressure begins to increase again at an axial location of 0.54, reattachment cannot be confirmed at this location with this current data. Downstream of this location is the viewing window for optical measurements; static pressure taps were not installed in this area at the time of this study. Towards the exit of the diffuser the data shows the static pressure did continue to increase, but is beginning to come back down at it enters the constant cross-section, circular rake case.

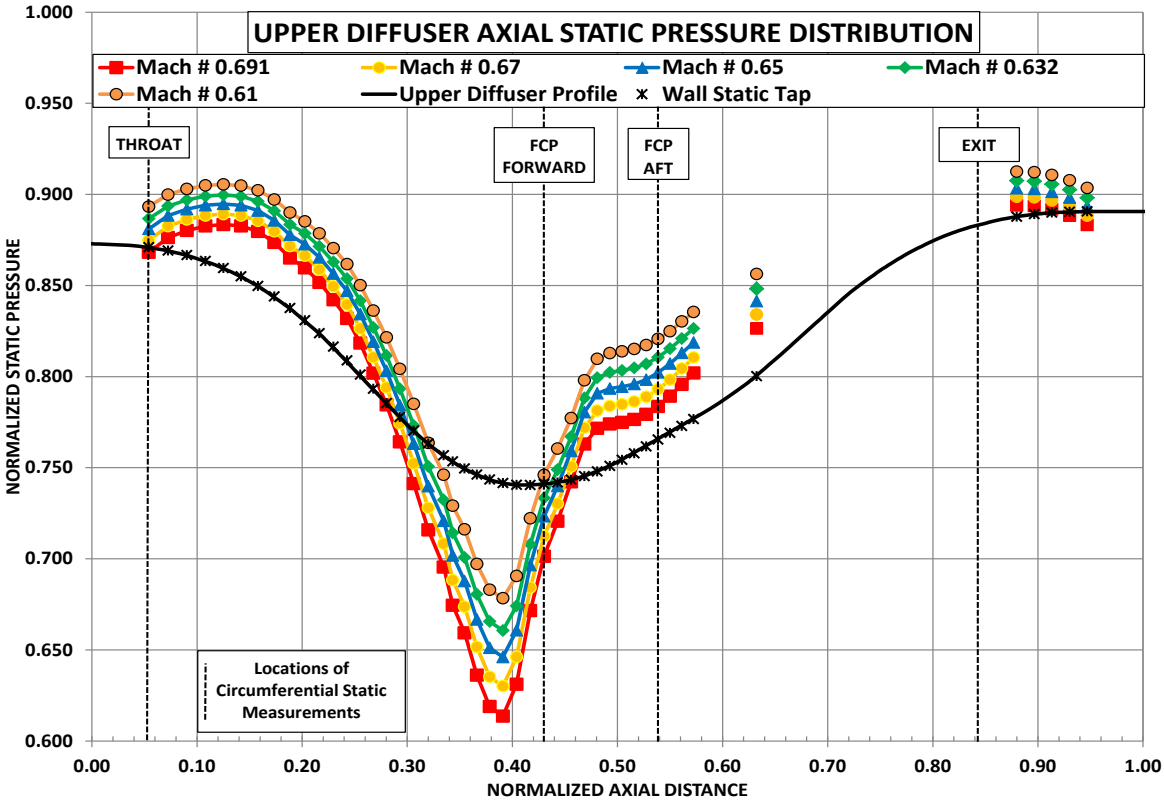

Figure 9. Axial static pressure distribution on the upper diffuser surface

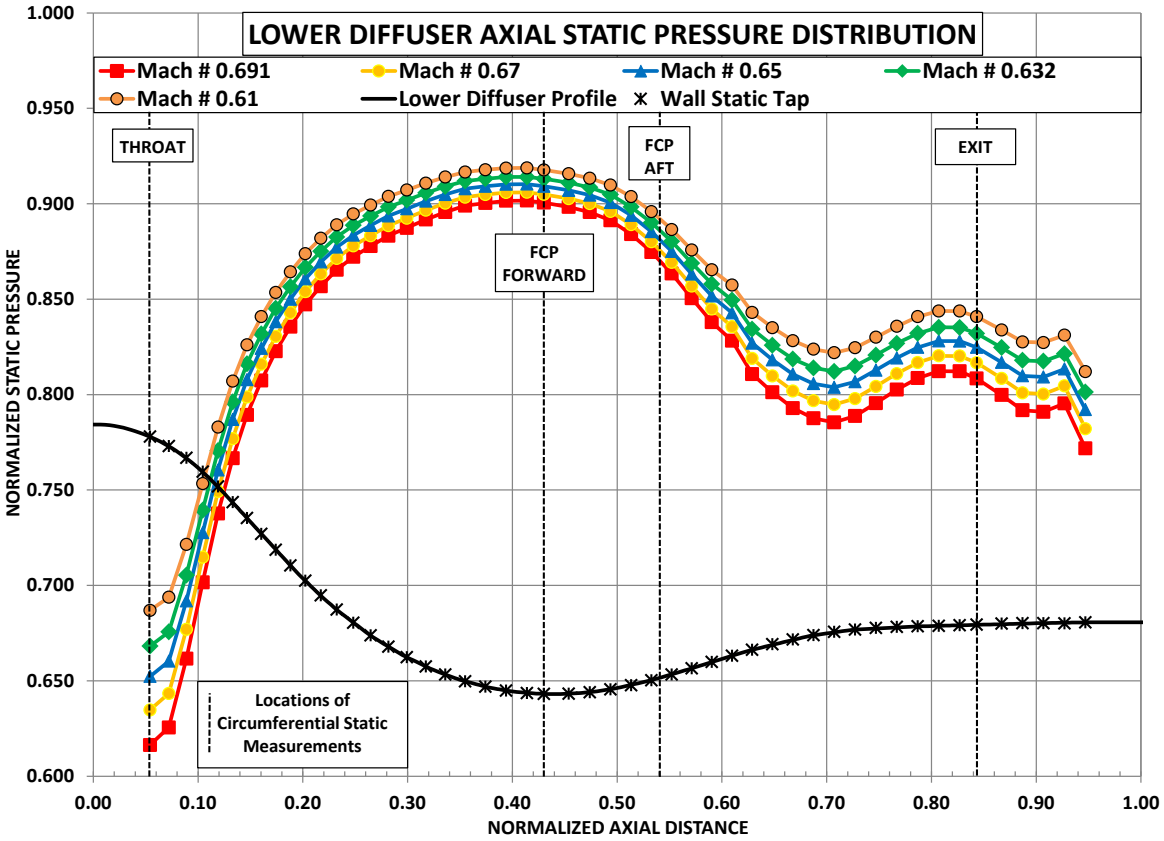

Figure 10. Axial static pressure distribution on the lower diffuser surface

The static pressure profile from the lower surface of the diffuser shown in Figure 10 appears to contain no separation region as indicated by the smooth and continuous profile. Overall, the static pressure behaves in a similar fashion as the upper surface. The flow enters the diffuser and is immediately turned downward. The lower surface is on the inside of the turn and displays an adverse pressure gradient up until the middle of the second turn. At this point the diffuser geometry has turned the flow back upward, and the lower surface is now on the outside of the turn and displays a favorable pressure gradient. There is no indication from the static pressure data on the lower surface that it was affected by the flow separation on the upper surface. The static pressure continues to decrease along the surface of the second turn up until nearly the end of the third turn, which turns the flow back axially. At this point the static pressure demonstrates a swing in the pressure gradient as it comes through the small curvature at the end of the duct. It is noted that the variation in cross-sectional shape along the duct is greater towards the discharge.

The effect of Mach number on both static pressure profiles is a downward shift due to the increased velocity. For the Mach numbers tested here and the data presented, there does not appear to be an effect on the location or the extent of the separation. Again, although the Mach number was varied, its change in Reynolds number was minimal and it is expected that the Mach number variation would have little impact on the flow physics.

Figure 11 is a plot of the difference in the static pressure on the upper and lower surface of the diffuser. A linear interpolation of static pressure was used in this calculation so that the difference in static pressure could be calculated at a common location. The purpose of this plot is to demonstrate the pressure gradient that exists between the upper and lower surfaces. A positive value on this plot indicates the upper surface has a higher static pressure and its magnitude is an indication of the potential of the low momentum fluid on this top surface to translate out and around to the lower pressure bottom surface. This plot also shows the locations where the difference in static pressure between the two surfaces becomes neutral. This occurs at an axial distance of 0.21 and 0.62. It is noted that the separation along the top surface occurs just downstream of the maximum static pressure difference between these two surfaces. At this location there is a large potential for the low momentum fluid on the bottom surface to translate around to the top surface, effectively increasing the boundary layer thickness and providing favorable conditions for separation.

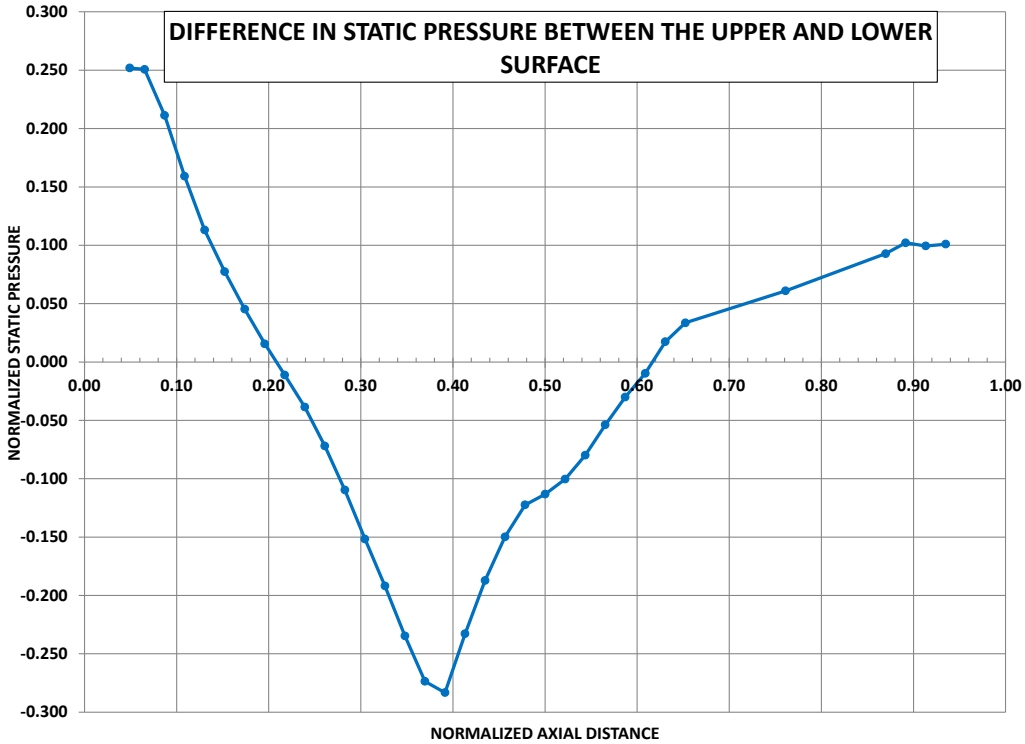

Figure 11. Axial static pressure difference between upper and lower diffuser surface

Figures 12-14 are of the circumferential static pressure distribution located at: the entrance of the flow control plug, exit of the flow control plug, and near the exit of the diffuser. The location of the measurement plane for Figure 12 is located just downstream of the middle of the second turn and just upstream of the axial separation

location. Wall statics wrap completely around the diffuser flow surfaces at this measurement plane. The profile is symmetric and gives an indication of the circumferential pressure gradient that is present and the potential for secondary flow to exist. This measurement plane does show three points on the upper surface of constant static pressure, but it is not clear if this is indicative of the downstream separation. In comparison to the circumferential static pressure profile at the experimental throat (figure 8), the profile is flipped in that the upper surface contains the region of low static pressure relative to the lower surface. This reversal of the static pressure gradient is due to the centerline curvature of the diffuser geometry and upper surface changing from being on the outside of the first turn and then the inside of the second turn and vice versa for the lower surface.

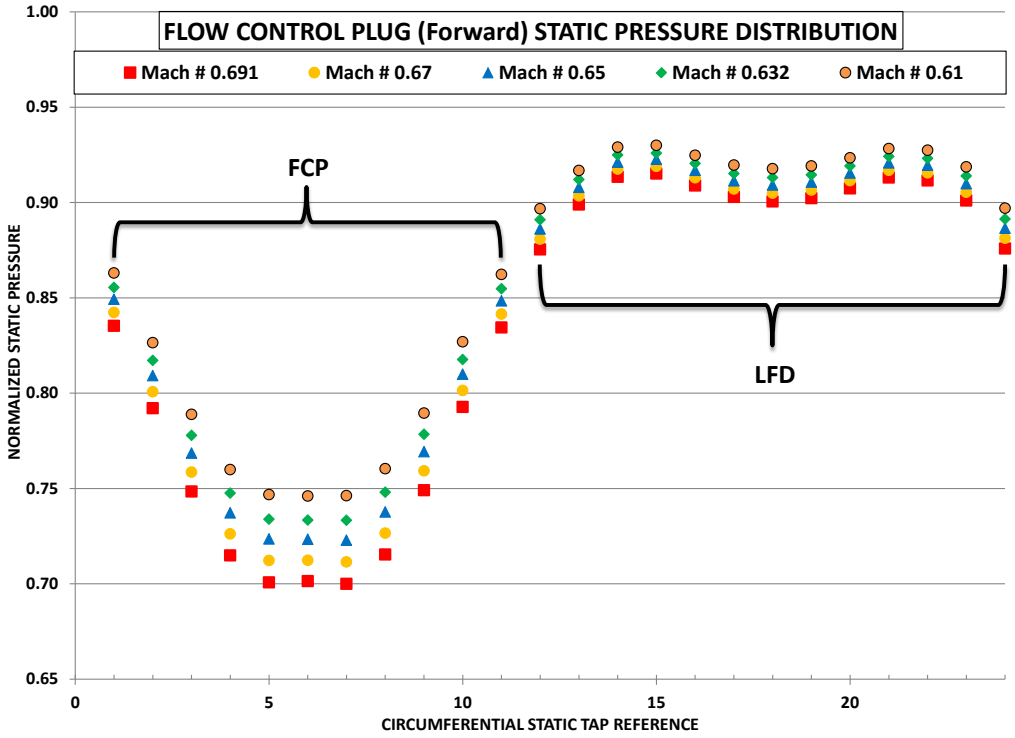

Figure 12. Circumferential static pressure distribution near the entrance of the flow control plug

The location of the measurement plane depicted in Figure 13 is just downstream of the separation region indicated on the axial static pressure distribution in Figure 9. This measurement plane only includes wall statics along the upper surface of the diffuser within the flow control plug. As mentioned earlier, it is not clear if the flow has reattached at this point. The static pressure profile shows a symmetric distribution of static pressure with the lowest pressure located at the center. Although not much can be concluded from these two circumferential distributions in terms of flow separation, these measurement planes will be very beneficial with the application of flow control in future studies.

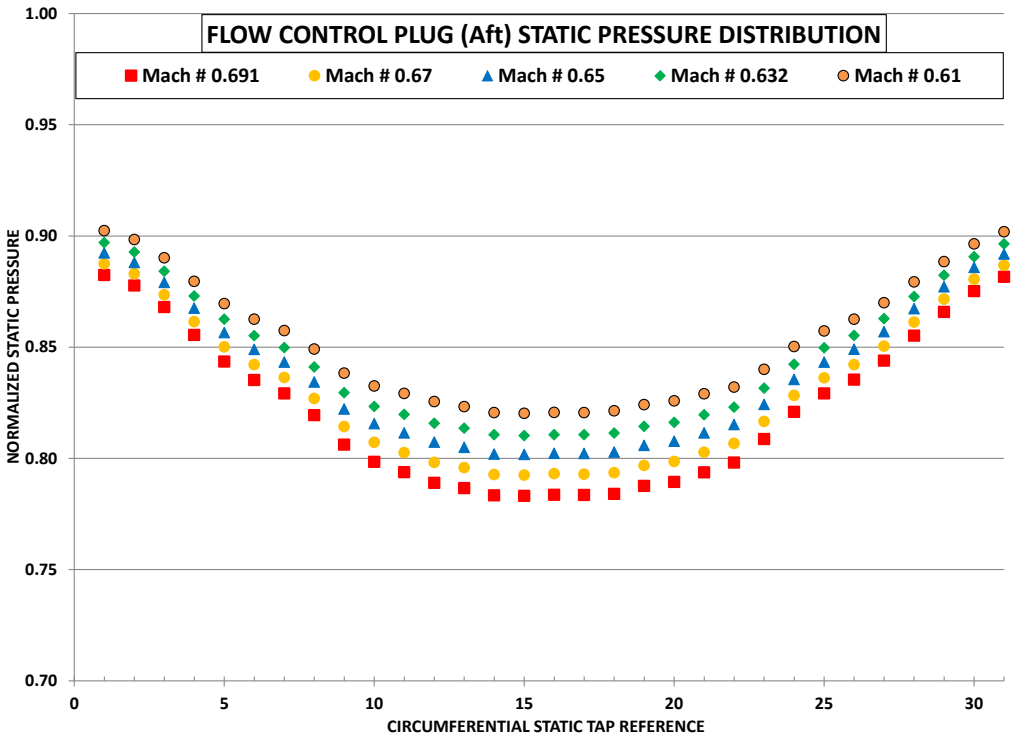

Figure 13. Circumferential static pressure distribution on the upper surface of the flow control plug

Figure 14 shows the circumferential wall static pressure distribution near the exit of the diffuser. The profile along the upper surface (outside turn) is reversed to that in Figure 12 which is located on the inside of the turn. The degree of turning along the bottom surface at this location is minimal, which has resulted in a decrease in the pressure difference between the two surfaces.

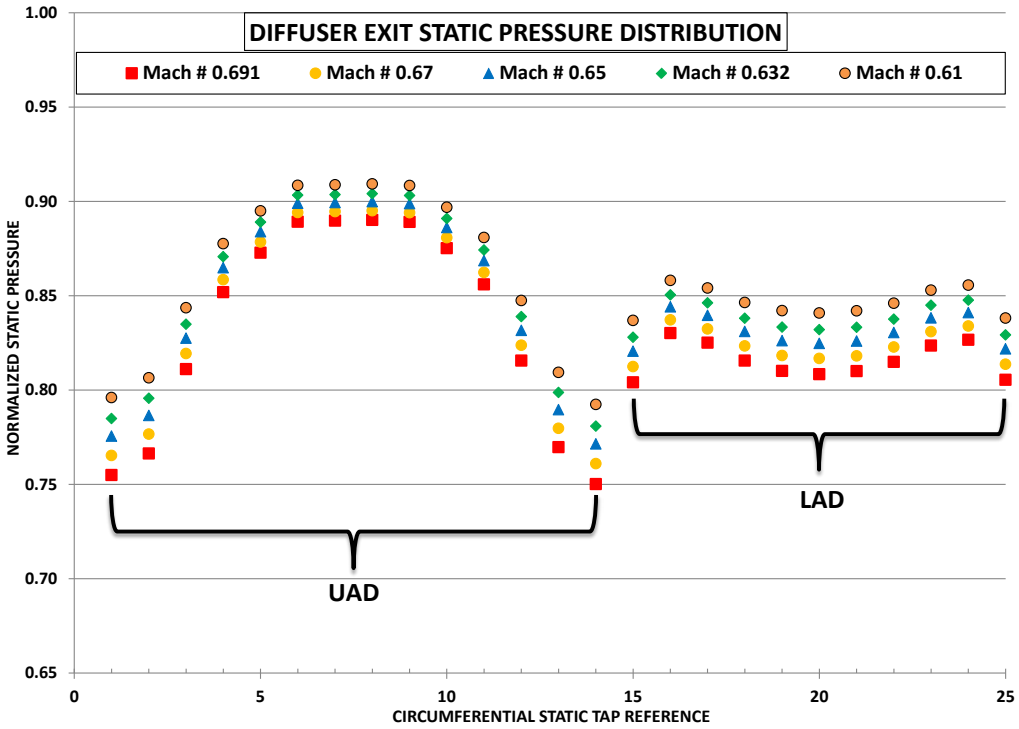

Figure 14. Circumferential static pressure distribution at a plane near the exit of the diffuser

B. AIP Measurements

Measurements were made at the AIP through a well instrumented steady pressure rake case described above. The data presented here is for a Mach number of 0.691 based on wall statics at the experimental throat and the inlet total pressure. All pressure measurements are normalized with respect to the inlet total pressure. In order to get the resolution presented in the figures below, the diffuser flow path was rotated with respect to the fixed exit rakes as described previously. Again this resulted in the equivalent of 721 total pressure measurements, and 72 wall static measurements.

Figure 15 shows the circumferential static pressure distribution at the AIP and contains repeat points to demonstrate the repeatability of the measurement. The distribution is symmetric, but still contains a significant amount of variation even though the cross-section is completely circular. The point of the lowest static pressure is located near the bottom of the duct and the highest static pressure is located at the top of the duct. This indicates that a potential is still present at the AIP for secondary flow to exist.

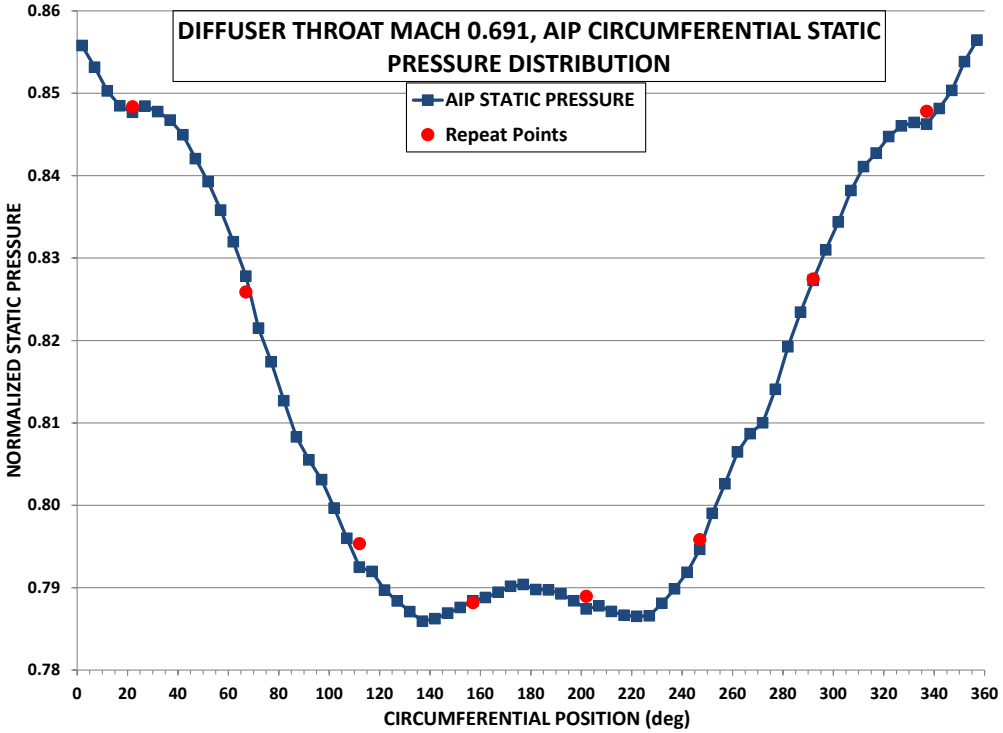

Figure 15. Circumferential static pressure distribution at the AIP

The five circumferential static pressure profiles along with the axial static pressure profiles presented show the presence of a static pressure gradient between the two surfaces. This gradient reverses several times as the upper and lower surface transitions from being on the outer and inner bends of the centerline curvature of the duct. The presence of this gradient gives an indication that secondary flow is present within the flow field. The extent of the secondary flow was not measured in the current investigation, but was shown to exist in the corresponding computational efforts [15-16]. The effect of this secondary flow is apparent in the AIP total pressure profiles shown below. Work done by Detra [17] and other investigators, have shown that the secondary flow results from the core flow having a higher velocity and therefore acted upon with a higher centrifugal force (relative to the fluid near the walls) induced by the curvature of a bend. The higher centrifugal force on the core flow pushes the fluid to the outer wall, which displaces the slower moving boundary layer fluid out and around and accumulates on the wall of the inside of the bend. The investigations on typical S-ducts cited previously have shown this accumulation of the boundary layer fluid which, as a result of the increased vorticity induced by the secondary flow, can roll up into a pair of counter-rotating vortices. This correlation is used here to describe the source of the pressure deficits shown in the total pressure contours.

A contour plot of the steady state total pressure measured at the AIP is shown in Figure 16. The profile indicates there is a large, localized total pressure deficit at the top of the exit of the diffuser. This deficit at the AIP is seen in

similar investigations of typical S-ducts and has been shown to be a function of a counter-rotating vortical structure [3, 6-9]. The parallel computational effort performed by Sanders et al [16], shows this top pressure deficit is in fact due to a pair of counter-rotating vortices that formed from the upper surface just downstream of the separation. In addition to this, there were three other localized pressure deficits visible at the AIP. Two were located along the sides of the plane and one was located at the bottom. Again from previous studies and the parallel computational effort, the two deficits along the side have been shown to be caused by another set of counter-rotating vortices that are weaker in strength due to being formed earlier in the duct. The low pressure region along the bottom of the profile is assumed to be a function of the increased boundary layer due to the secondary flow described earlier. At the core of this profile, there is very little total pressure deficit. The size of this core contributes to the overall total pressure recovery of the duct of 0.983. Although the duct has a reasonable recovery factor, the intensity of the secondary flow, or vorticity, was not quantified and could pose issues to the compression system.

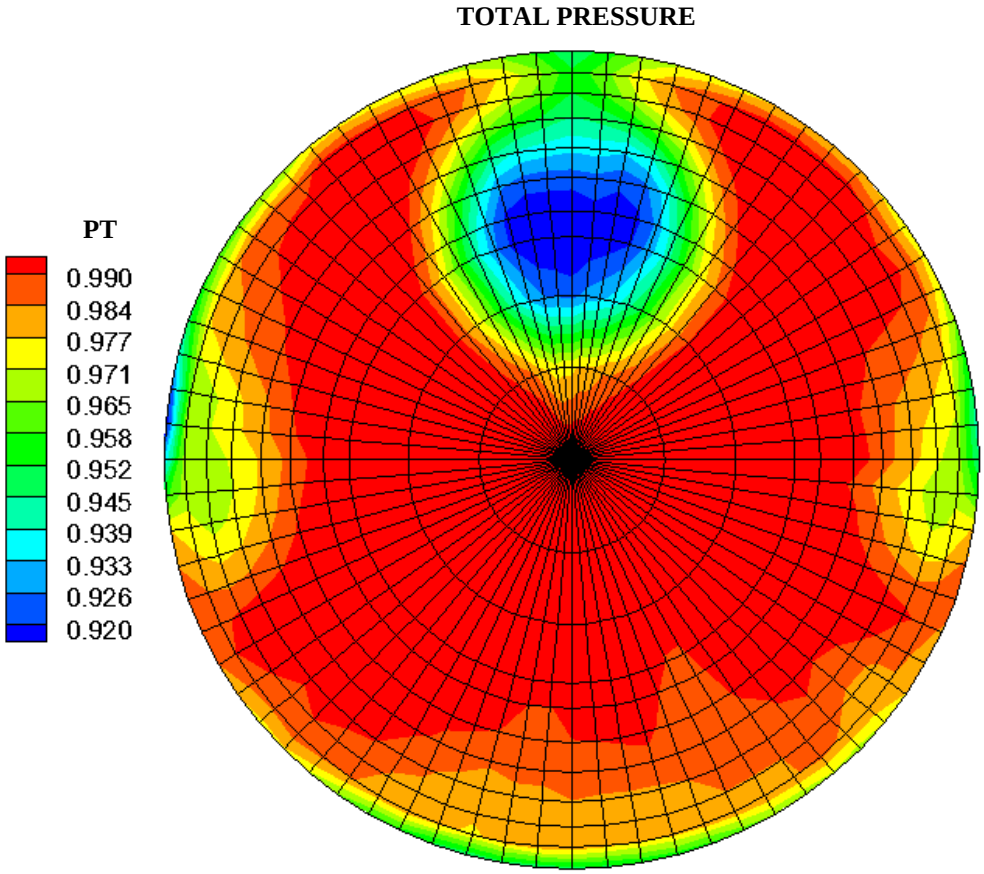

Figure 16. Total pressure contour with measurement grid overlaid

An approximate diffuser exit Mach number contour plot was calculated using the AIP wall static pressure data. Since the total pressure rakes were not capable of measuring static pressure, an approximation was made to calculate the static pressure at each probe location. The approximation was performed by using the average of all the wall static pressures and interpolating from the center outward using this average static pressure to each static pressure measured at the wall. The resulting Mach number contour plot is shown in Figure 17. This contour plot agrees with the exit design Mach number and what was expected at the exit of the diffuser given the total pressure profile.

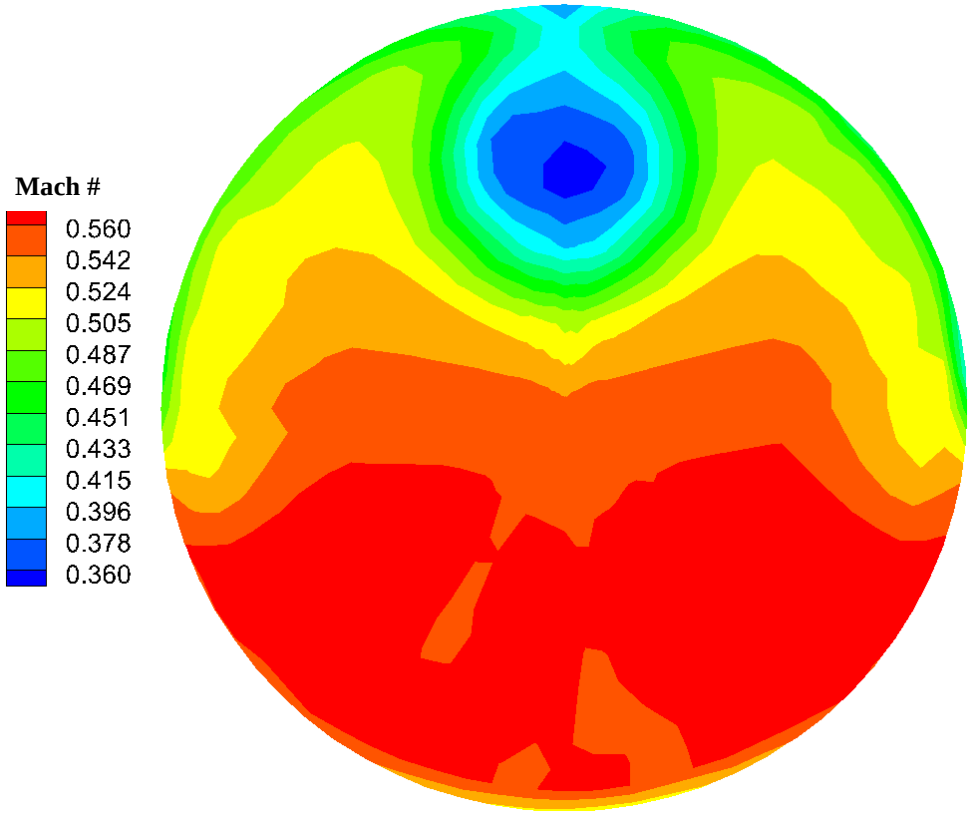

Figure 17. Diffuser exit Mach number

The Society of Automotive Engineers (SAE) has formed a subcommittee (S-16) to establish methodologies to characterize inlet distortion and quantify it with respect to its effect on compressor performance. These methodologies are outlined in the Aerospace Recommended Practice (ARP) 1420 document and quantified using distortion descriptors. More recently, the SAE S-16 subcommittee has published an Aerospace Information Report (AIR) 5686 to standardize a methodology for assessing inlet swirl [18], which is expected to be more prevalent in serpentine diffusers. Swirl data was not acquired in this current investigation but is planned to be in future studies.

With the data obtained from the steady state total pressure rake case, the distortion extent, intensity, multiple per-rev content, and the radial intensity were calculated and are presented in the tables below. This data is presented for reference but cannot be characterized without further investigation or modeling of the compression system. This will be undertaken in a future study.

	$\left(\frac{\Delta PC}{P}\right)$	ϑ^{-}	MPR	$\left(\frac{\Delta PR}{P}\right)$
Ring 1 (hub)	0.0121	86.6	1.00	-0.01251
Ring 2	0.0390	83.1	1.00	-0.00432
Ring 3	0.0482	80.1	1.00	-0.00179
Ring 4	0.0488	73.6	1.00	-0.00121
Ring 5	0.0439	66.0	1.00	-0.00082
Ring 6	0.0350	57.2	1.04	-0.00073
Ring 7	0.0297	46.1	1.42	-0.00042
Ring 8	0.0270	33.6	2.51	0.00047
Ring 9	0.0275	27.4	2.82	0.00179
Ring 10 (tip)	0.0253	47.3	2.26	0.01953

Table 1. Distortion descriptors by ring

	$\left(\frac{\Delta PC}{P}\right)$	ϑ^-	MPR	$\left(\frac{\Delta PR}{P}\right)$
Face Average	0.0335	60.9	1.51	0.0000

Table 2. Distortion descriptors averaged for all of the rings

IV. Conclusion

Data was presented from an ongoing Phase I effort of an extensive research program to identify the influence of serpentine diffusers when they are close coupled to transonic fans for short embedded airframe designs. Further research will detail the influence of pressure distortion of this nature on the fan, along with a relatively new parameter of interest: inlet swirl. It is envisioned that these results will aid in evaluating how the fan and diffuser interact in a coupled configuration.

Axial and circumferential wall static pressure data was presented at various locations throughout the diffuser. It was shown that a pressure potential exists throughout the duct for secondary flow to be established. The diffuser geometry under investigation displayed separated flow along the upper surface for all five Mach numbers tested. Circumferential pressure profiles gives insight to the complex 3-dimensional flow that was present in this diffuser.

Full contour plots of total pressure and Mach number at the AIP were presented along with calculated distortion descriptors. The profile indicates there was a large, localized, total pressure deficit at the top of the exit of the diffuser. In addition to this, there were three other localized pressure deficits visible at the AIP. From previous studies and a parallel computational effort, the large pressure deficits were assumed to be a result of counter rotating vortical structures formed within the duct. The low pressure region along the bottom of the profile was assumed to be a function of the accumulation of boundary layer fluid due to secondary flow. At the core of this profile, there was very little total pressure deficit. The size of this core contributes to the overall total pressure recovery of the duct of 0.983.

Acknowledgments

The authors wish to acknowledge the assistance provided by the Aerospace Systems Directorate Integration Branch, Dr. Angie Scribben, and Mr. Matt Goettke. In addition the authors acknowledge the design work by Mr. Joseph Hall of Virginia Tech in developing the ACF and the efforts of both Tri-Models Inc., and Virginia Tech for developing the research article and the steady-state rake case respectively. Finally the authors would like to acknowledge the assistance provided by Dr. Darius Sanders related to Computational Studies used to help guide the experiment and all the other members of the Turbomachinery Branch, Compressor Aero Research Lab research team for their advice and assistance in completing this phase of the research program.

V. References

[1]Vakili, A., Wu, J.M., Liver, P., and Bhat, M.K., 1983, "Measurements of Compressible Secondary Flow in a Circular S-Duct," AIAA 83-1739.

[2]Bransod, P., and Bradshaw, P., 1972, "The Flow in S-shaped Ducts," The Aeronautical Quarterly, Volume 23.

[3]Wellborn, S.R., Reichert, B.A., and Okiishi, T.H., 1992, "An Experimental Investigation of the Flow in a Diffusing S-Duct," AIAA/SAE/ASME/ASEE 28th Joint Propulsion Conference and Exhibit, AIAA-92-3622.

[4]Taylor, A.M.K.P., Whitelaw, J.H., and Yianneskis, M., 1984, "Developing Flow in S Shaped Ducts II – Circular Cross-Section Duct," NASA Contractor Report 3759.

[5]Rowe, M., 1970, "Measurements and Computations of Flow in Pipe Bends," Journal of Fluid Mechanics, Volume 43 Part 4, pp.771-783.

[6]Towne, C.E., 1984, "Computation of Viscous Flow in Curved Ducts and Comparison with Experimental Data," AIAA 22nd Aerospace Sciences Meeting, AIAA-84-0531.

[7]Vakili, A., Wu, J.M., Hingst, W.R., and Towne, C.E., 1984, "Comparison of Experimental and Computational Compressible Flow in a S-Duct," AIAA 22nd Aerospace Sciences Meeting, AIAA-84-0033.

[8]Harloff, G. J., Reichert, B. A., and Wellborn, S.R., 1992, "Navier-Stokes Analysis and Experimental Data Comparison of Compressible Flow in a Diffusing S-duct" AIAA 10th Applied Aerodynamics Conference

[9]Rabe, A. C., "Effectiveness of a Serpentine Inlet Duct Flow Control Scheme at Design and Off-Design Simulated Flight Conditions," Ph.D. Dissertation, Virginia Tech, 2003.

[10]SAE S-16 Committee, 1998, ARP 1420, "Gas Turbine Engine Inlet Flow Distortion Guidelines," Society of Automotive Engineers.

[11]Society of Automotive Engineers. “Inlet Total-Pressure-Distortion Considerations for Gas-Turbine Engines,” Aerospace Information Report AIR1419, Rev. B, 2007.
[12] Description of AFRL exhauster capability http://www.wpafb.af.mil/shared/media/document/AFD-070425 062.pdf CRAF description
[13] Gracey, W., NACA Report 1303, “Wind-Tunnel Investigation of a Number of Total-Pressure Turbes at High Angles of Attack Subsonic, Transonic, and Supersonic Speeds, Page 503, 1957.
[14]Schlichting, H., 1955, Boundary-Layer Theory, McGraw Hill Book Company.
[15]Sanders, Darius D., and List, Michael G., "Simulation of Distortion Generation in a Modern Serpentine Diffuser to Improve Experimental Effectiveness," Proceedings of the 2012 DoD HPCMP Users' Group Conference, June 2012. (Accepted by ITEA Journal of Test and Evaluation, Oct. 2012).
[16]Sanders, Darius D., and List, Michael G.," CFD Performance Predictions of a Serpentine Diffuser Configuration in an Annular Cascade Facility,” 51th AIAA Aerospace Sciences Meeting & Exhibit, AIAA Paper, (submitted for publication).
[17]Detra, W. “The secondary flow in curved pipes,” Ph.D. Dissertation, Swiss Federal Institute of Technology, Zurich, 1953
[18] Society of Automotive Engineers, “A Methodology for Assessing Inlet Swirl Distortion,” AIR5686, 2010.